Solar Physics
DOI: 10.1007/•••••-•••-•••-••••-•

Sympathetic Quiet and Active Region Filament Eruptions

Kostadinka Koleva[1] · Pooja Devi[2] · Ramesh Chandra[2] · Reetika Joshi[2] · Peter Duchlev[3] · Momchil Dechev[3]

Abstract We present the observations of three sympathetic filament eruptions occurring on 19 July 2015 namely F_1, F_2, and F_3. The events were observed in UV/EUV wavelengths by Atmospheric Imaging Assembly onboard the Solar Dynamics Observatory and by Global Oscillation Network Group telescope in Hα line. As filament F_1 starts to erupt, a part of it falls close to the location of the F_2 and F_3 filaments. This causes the eruption of F_2 and F_3 during which the two filaments merge together and trigger a medium-class CME and a long-duration GOES C2.1 class flare. We discuss the dynamics and kinematics of these three filament eruptions and related phenomena.

Keywords: Sun - flares: Sun - filament eruptions: Sun - magnetic fields

✉ Kostadinka Koleva
kkoleva@space.bas.bg

Pooja Devi
setiapooja.ps@gmail.com

Ramesh Chandra
rchandra.ntl@gmail.com

Reetika Joshi
reetikajoshi.ntl@gmail.com

Peter Duchlev
duchlev@astro.bas.bg

Momchil Dechev
mdechev@astro.bas.bg

[1] Space Research and Technology Institute, Bulgarian Academy of Sciences, Bulgaria

[2] Department of Physics, DSB Campus, Kumaun University, Nainital 263 002, India

[3] Institute of Astronomy and NAO, Bulgarian Academy of Sciences, Bulgaria

1. Introduction

Solar filaments/prominences are well-known phenomenon in the solar atmosphere. They present a variety of cool and dense objects, ranging from long-lived quiescent filament/prominence to short-lived active region filament/prominence. Their nature is described in many studies (van Ballegooijen and Martens, 1989; Chae, 2001; Labrosse *et al.*, 2010; Mackay *et al.*, 2010; Schmieder, Démoulin, and Aulanier, 2013; Gibson, 2018). It is believed that they are supported in magnetic dips (Aulanier, DeVore, and Antiochos, 2002; Mackay *et al.*, 2010; Gibson, 2018), observed on polarity inversion line (PIL).

When the balance between magnetic pressure and magnetic tension in the filaments becomes unstable by any kind of mechanism, they can erupt. Observations show that based on the relation between the filament mass and corresponding supporting magnetic structure filaments can erupt fully (Gopalswamy *et al.*, 2003; Schrijver *et al.*, 2008; Chandra *et al.*, 2010) or partially (Gibson and Fan, 2006; Joshi *et al.*, 2014; Cheng, Kliem, and Ding, 2018; Monga *et al.*, 2021) and sometimes the eruption can be failed (*e.g.,* Liu, Wang, and Alexander, 2009; Kumar *et al.*, 2011; Joshi *et al.*, 2013). The full or partial eruption are usually associated with the coronal mass ejections (CMEs), which later on become Interplanetary CME (ICME), responsible for space weather disturbances (Gopalswamy, Yashiro, and Akiyama, 2007; Schmieder *et al.*, 2020).

Sometimes, merging of the filaments is also observed (Schmieder *et al.*, 2004; Chandra *et al.*, 2011; Jiang *et al.*, 2014; Luna *et al.*, 2017). Merging can tell us about the formation and the dynamical evolution of the filaments. Cases are reported, where two filaments merge and the result can be stable or eruptive filament. Such phenomena were simulated in high beta plasma condition by Linton (2006) and in low beta plasma coronal condition by Aulanier, DeVore, and Antiochos (2006) and Török *et al.* (2011). In Addition to it laboratory experiment has also been performed (Gekelman, Lawrence, and Van Compernolle, 2012).

Occasionally, the eruptions occur in a short interval of time at same or different locations on the solar surface (Biesecker and Thompson, 2000; Moon *et al.*, 2002; Wang *et al.*, 2002; Zhukov and Veselovsky, 2007; Liu, Wang, and Alexander, 2009). The consecutive eruptions, occurring in the same active region within a relatively short time interval, are defined as sympathetic eruptions. Other cases could also be recognized as sympathetic eruptions, such as the recurring/successive eruptions that appear at different locations of the solar surface. Such events can occur in both quiet and active regions (Moon *et al.*, 2002; Wheatland and Craig, 2006; Schrijver and Title, 2011). Sympathetic eruptions have already been observed in the past (Richardson, 1936, 1951; Becker, 1958) and it is believed that they can be physically connected by the coronal loops. It was found that in case of sympathetic eruptions, the multiple flux systems erupt. First, the eruption starts in one active region, pushing the overlaying magnetic flux and causing other flux systems to erupt (Delannée and Aulanier, 1999; Wang *et al.*, 2002; Liu, Webb, and Zhao, 2006; Zhukov and Veselovsky, 2007). Another possibility was suggested by Khan and Hudson (2000). According

to them, the propagation of EUV waves can destabilize the adjacent loop system and ultimately lead to another eruption.

The sympathetic eruptions were modelled in MHD numerical simulations. Ding, Hu, and Wang (2006) performed the 2.5 D time-dependent MHD model. In this model they scrutinized the catastrophic behavior of a multiple flux rope system, which contains three magnetic flux ropes in three sets of separate loop arcades. They concluded that the eruption of the first flux rope disturbed the stability of the second and third flux ropes and forced them to erupt. According to the model proposed by Wheatland and Craig (2006), if a flare occurs in the location of a separator, it temporary increases the probability of flaring at all separators (a complex of reconnecting structures). Recently Török *et al.* (2011) presented 3 D MHD simulation of two magnetic flux ropes and reproduced the 2010 August 1 quiet filament eruptions. Their results support the hypothesis that the trigger mechanisms of sympathetic eruptions can be related to the large-scale coronal magnetic field. Despite the numerous observations and simulations, the exact reason for the sympathetic eruptions is still not well understood.

In this paper we present the observations of three sympathetically erupting filaments. Each eruption was associated with a CME. In addition to this, the observations also show the merging of two filaments. The paper is organized as follows: Section 2 describes the data sets used in the study. The results of our analysis are presented in Section 3. Finally, the discussion and summary of the investigation are presented in Section 4.

2. Observational Data Sets

For this study, we used the data from following sources:

1. **SDO/AIA data:** For the evolution and dynamics/kinematics study of the filament eruptions, we used data from the Atmospheric Imaging Assembly (AIA; Lemen *et al.*, 2012) onboard the Solar Dynamics Observatory (SDO; Pesnell, Thompson, and Chamberlin (2012)). The AIA consists of seven Extreme Ultra-Violet (EUV) and three Ultra-Violet (UV) channels which probe the solar corona with a pixel resolution of $0.6''$ and an average cadence of 12 s. The AIA image field-of-view (FOV) reaches 1.3 solar radii. For the present study we used 1 min cadence data from the AIA 171, 193 and 304 Å channels.

2. **Hα Data:** Hα images from Global Oscillation Network Group (GONG; Harvey *et al.*, 1996) were used to study the chromospheric evolution of filament eruptions. GONG observes the full Sun in Hα with a cadence of 1 min and a pixel resolution of $1''$.

3. **SDO/HMI magnetic field data :** The line-of-sight magnetograms taken by Helioseismic and Magnetic Imager (HMI; Scherrer *et al.*, 2012; Schou *et al.*, 2012) on board SDO were used to explore the photospheric magnetic fields configuration in the corresponding regions. The HMI LOS magnetograms used in this study have a cadence of 10 min and pixel size of $0.5''$. The 1σ noise

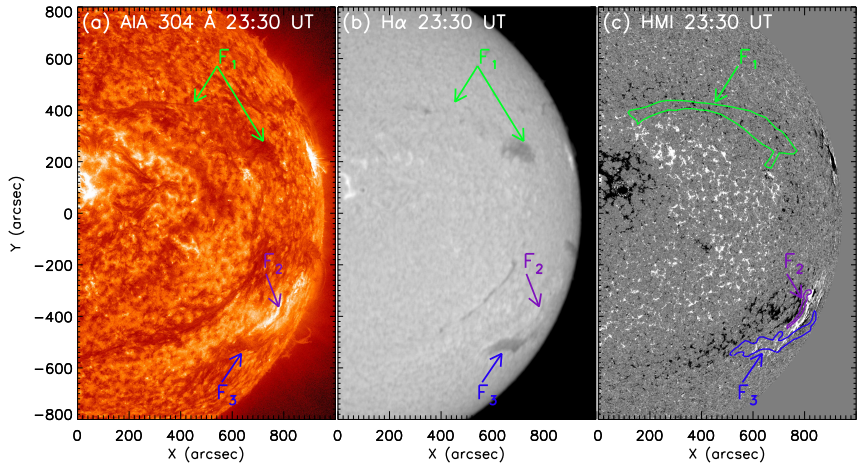

Figure 1. Three visible filaments in AIA 304 Å (panel a) and Hα (panel b) on 18 July 2015. The contours of 304 Å filaments F_1, F_2, and F_3 are over-plotted over HMI magnetogram (panel c) with green, purple, and blue colors, respectively.

level for HMI line-of-sight magnetogram is 10 G (Liu *et al.*, 2012). The HMI magnetograms and AIA images were co-aligned by using the UV AIA 1600 Å images, which was consequently aligned with the AIA EUV channels. All data were corrected for projection effect and derotated to 23:20 UT on 18 July 2015.

4. **LASCO CME data:** The CME association of the erupted filaments was traced in the field-of-view (FOV) of the C2 Coronagraph (2.2 – 6 $R_\odot$) of Large Angle and Spectrometric Coronagraph (LASCO; Brueckner *et al.*, 1995) on board the SOHO satellite.

3. Results

On 19 July 2015, three filaments erupted sympathetically. First one was a quiescent filament, while the other two filaments were situated in an active region. The dynamics and the kinematics of these eruptions are presented in the following sub-sections.

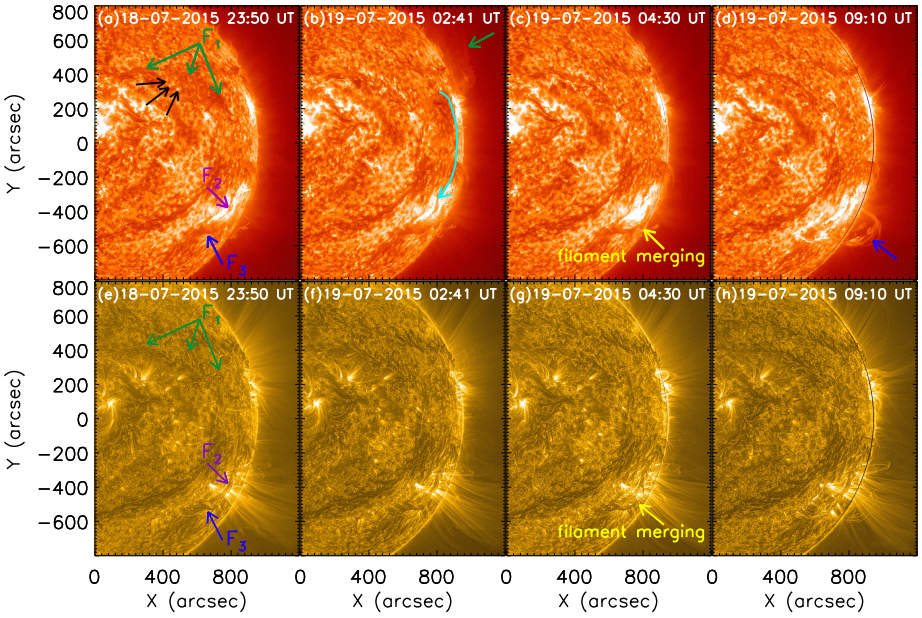

Figure 2. Evolution of the event in AIA 304 Å and 171 Å wavelength in top and bottom rows, respectively. Panels (a) and (e) show the filaments F_1, F_2, and F_3 with green, purple, and blue arrows, respectively. Panel (b) shows the erupting filament F_1 with green arrow and cyan arrow shows the filament material falling downward (towards filament F_2), which triggers the filament F_2 (panel d). The yellow arrow in panels (c) and (g) is pointing the merging of filaments F_2 and F_3. The AIA 171 Å images are processed with MGN method. The black arrows in panel (a) shows the pre-eruptive brightening in the vicinity of filament F_1. The Movies of these data are available in the Electronic Supplementary Materials.

3.1. Dynamics

We named the three filaments as F_1, F_2, and F_3 respectively. Filament F_1 was located in northern hemisphere, on the other hand filaments F_2, and F_3 were located in southern hemisphere. The location of all these three filaments are shown in panels 'a' and 'b' of Figure 1 in AIA 304 Å and Hα respectively. In panel 'c' of the figure the AIA 304 Å filament contours are overlaid on photospheric magnetic field by green, pink and blue colours. This image was obtained before the eruption on 18 July 2015. Filament F_1 was a large filament (projection length $\sim$ 450 Mm) that was observed on the solar disk between 11 – 19 July 2015. It survived around eight days on solar disk and erupted on 19 July 2015. The filaments F_2 and F_3 were located in the NOAA active region (AR) 12384. Initially these filaments were observed as a single filament up to 16 July 2015, which on 17 July 2015 splitted into two smaller parts as earlier named as F_2 and F_3.

Figure 2 illustrates the filament eruption evolution in AIA 304 Å and 171 Å wavelengths in top and bottom rows, respectively. To make the evolution more clear, we have created the MGN processed images in 171 Å. This method is proposed by Morgan and Druckmüller (2014). It is based on the localized

normalization of the data at different spatial levels. There are several parameters in this code, which can be changed according to the waveband *namely* 'γ' , 'k', 'h'. The 'γ' parameter is useful for the global gamma transformation of the image, the parameter 'k' controls the sharpness of the gamma transformation and 'h' is the approximate weight of the global normalized image. We used the original default values of 'γ' and 'k' described in the original code as 3.2 and 0.7, respectively. We modified slightly the value of 'h' to 0.9, as it can be changed for the type of input image and for the desired output. Before applying the MGN technique, firstly the AIA data is pre-processed using *aia_prep* procedure and all the images are aligned at a fixed time, to compensate the solar rotation effect, using *drot_map* routine available in SSWIDL. Such image processing is useful to present clearly the structural evolution of the eruption (Devi *et al.*, 2021). Here we discuss the eruption evolution of the filaments step-by-step. The filament F_1 started to rise $\sim$ 01:00 UT on 19 July 2015. The erupted material went into two major directions. Part of the erupted filament moved towards northwest direction. This erupted part became visible in LASCO C2 FOV as a CME at $\sim$ 03:36 UT with a speed of $\sim$ 126 km s^{-1}. As the filament erupted two parallel elongated brightening along the PIL, where the F_1 filament was situated before its eruptions, were observed. These two ribbons were very faint. We could not see any enhancement in the GOES X-ray flux at this time. This could be due to the weak reconnection occurrence during the filament eruption as illustrated in the study of Chandra *et al.* (2021).

Remaining part of the erupted F_1 filament advanced into south direction, as shown by cyan arrows in Figure 2. Finally it fell down towards the filament F_2 and reached up to its north feet (see Figure 2(b)). As a result filament F_2 started to rise and merged with filament F_3 around 04:33 UT. Part of the filament F_2 was skipped from the solar surface and appeared as a very faint CME at 05:24 UT in LASCO C2 FOV.

The merged filament started to rise slowly in southwest direction at $\sim$ 05:10 UT. This eruption was associated with a C-class GOES solar flare and a partial halo (width $\sim$ 194°) CME with a linear speed of $\sim$ 782 km s^{-1}, which was first observed in the LASCO C2 FOV at $\sim$ 09:48 UT at a height of $\sim$ 2.9 R_{sun}.

The chronology of these eruptions and related activities are presented in Table 1.

3.2. Kinematics

To investigate the temporal and spatial connection between the three erupted filaments, we performed the time-distance analysis. This technique is based on the exploration of the motion of plasma material along an artificial slit. For this purpose, we have selected different slits in some selected directions. These slits were named as S_1, S_2, S_3, and S_4 respectively.

The slit S_1 was selected in order to analyse the kinematic behavior of F_1 eruption in the north west direction. The selected slit and the corresponding

Table 1. Chronology of the eruptions.

Time (UT)	Activities	Notes
23:40* – 00:50	Activation of filament F_1	* time one day earlier
00:50 – 03:20	Part of F_1 material moved northwest	–
03:36	CME appearance in LASCO FOV	Related with northwest part
01:30 – 04:00	Part of F_1 material moved southward	Reached upto F_2
04:11	Activity in filament F_2	Partial eruption
04:33	Start of the merging of F_2 and F_3 filaments	–
04:33 – 05:10	Small oscillations in F_3	–
05:24	small CME in LASCO FOV	Related to F_2 partial eruption
05:00	Final merging of F_2 and F_3 filaments	
05:10	F_3 starts to rise	Small velocity (few km s^{-1})
07:00	F_3 starts faster velocity	velocity $\sim$ 12 km s^{-1}
09:00	F_3 acceleration phase	velocity $\sim$ 138 km s^{-1}
09:10	GOES C2 flare onset	Long duration flare ($\sim$ 7 hrs)
09:48	CME appearance in LASCO FOV	A partial halo CME

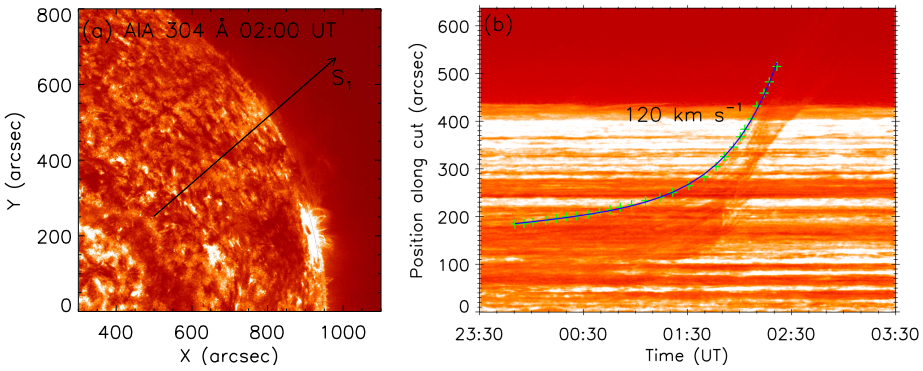

Figure 3. Panel (a) is the AIA 304 Å image from 19 July 2015 02:00 UT showing the direction of the slice S_1. Panel (b) shows the time-distance plot corresponding to the slice S_1. The green 'plus' symbols in panel (b) are the data points chosen from the time-distance plot and blue solid line is the fitting curve to these data points. The fitted function is $ae^{b(t-t_0)} + ct + h_0$. The eruption speed estimated from the fitting is found to be $\sim$ 120 km s^{-1}.

time-distance plot are shown in Figure 3. We have selected some points in the edge of the time-distance slice and overplotted them in the same image (Figure 3b) with 'plus' symbol in green color. Further, these data points were fitted by a combination of linear and exponential functions, namely $(ae^{b(t-t_0)}+ct+h_0)$, as done by Cheng *et al.* (2020). Where a, b, c, and h_0 are arbitrary constants and the time t_0 is fixed at 23:50 UT on 18 July 2015. The fitted function is plotted as blue solid line in panel 'b' of the Figure. The computed speed is $\sim$ 120 $\pm$ 6 km s^{-1}. To determine the exact start time of the eruption, we used the equation

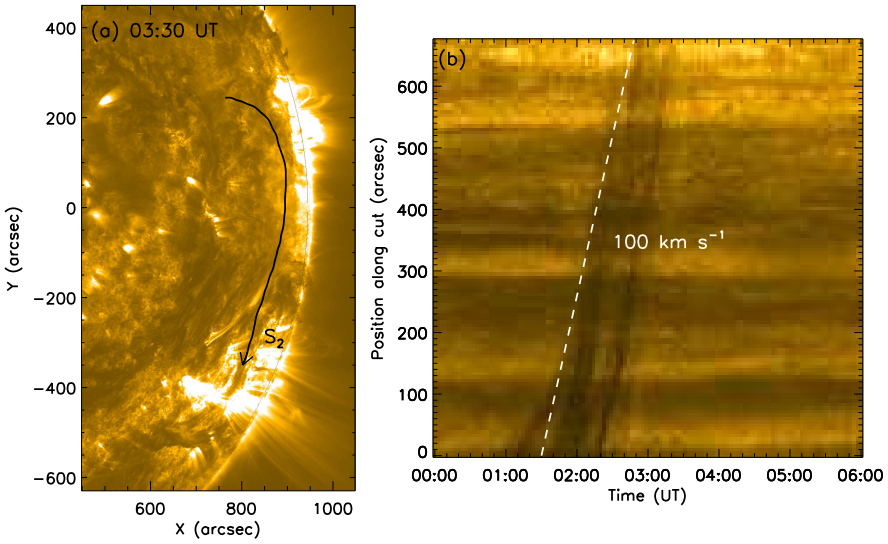

Figure 4. Panel (a): Image of AIA 171 Å on 19 July 2015 03:30 UT with the curved slice shown by black arrow, in the direction of the material falling from filament F_1 towards F_2. Panel (b): time-distance plot corresponding to the slice in panel (a).

$t_{start} = \frac{1}{b}\ln(\frac{c}{ab})$. According to our results the eruption started at $\sim$ 00:42 UT on 19 July 2015.

The slit S_2 was chosen at southward direction where part of F_1 material was observed to move. The slit position and the time-slice is depicted in Figure 4. The speed of material going in this direction was computed using the straight-line fit. The estimated speed value is about 100 ± 2 km s^{-1}, which is comparable but slightly slower than the speed of filament in north-west direction. This slower speed could be due to the following possibilities: Due to long curved path of S_2 along the closed loop channel (evidenced by the PFSS extrapolation in Figure 12), the material ejected from the filament F_1 decelerated and result as a slower speed. Another reason for the slower speed could be the expansion of the filament F_1. The erupting filament material reached the feet of filament F_2 at $\sim$ 03:20 UT.

The slit S_3 is placed between the filaments F_2 and F_3. The purpose of this slit is to comprehend the observed merging of these two filaments. The results are plotted in Figure 5. The time-distance plot indicates that the filament F_2 was in stationary state up to $\sim$ 04:10 UT and it started to rise at $\sim$ 04:20 UT. Around this time the filament F_2 became unstable due to the continuous flow of plasma material of F_1 filament. As a result the filament F_2 merged with F_3 at around 05:00 UT.

To examine the eruption of filament after merging, we have fixed the slit S_4 as shown in Figure 6. From the time-distance plot shown on the figure, it is evident that the eruption started at $\sim$ 05:10 UT, just after the F_2 and F_3 merging. Further from the image, it is noticeable that the eruption had three

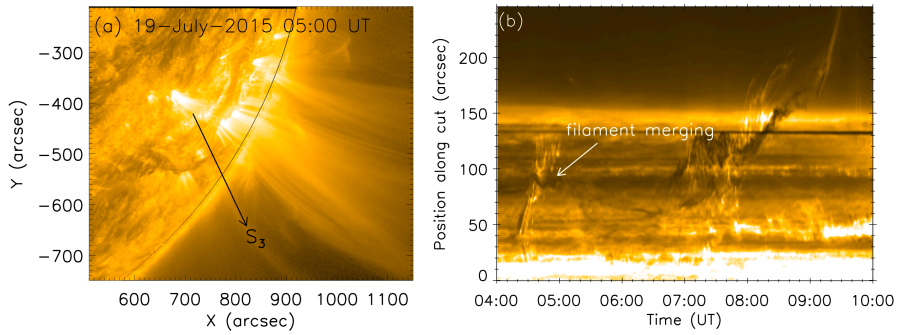

Figure 5. Image of AIA 171 Å showing the slice S_3 (panel a) and the time-distance plot corresponding to this slice in panel (b). The time-distance plot shows the merging of the filaments.

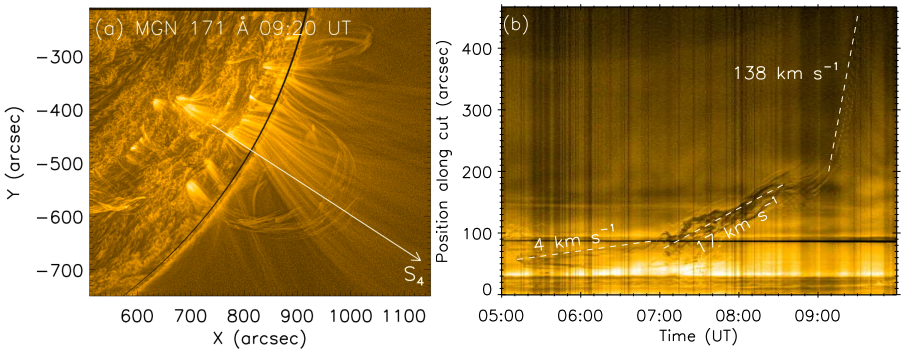

Figure 6. Panel (a): AIA 171 Å image, processed with the MGN, showing the slice S_4 which was taken in the direction of F_3 eruption. Panel (b): The time-distance plot of F_3 eruption, showing that it erupted in three phases with speeds of 4 km s^{-1}, 17 km s^{-1} and 138 km s^{-1}, respectively.

phases. The first phase, starting at $\sim$ 05:10 UT was a slow phase with a speed of $\sim$ 4 km s^{-1} and lasted up to 07:00 UT. After 07:00 UT the second phase started, where the eruption speed increased to about 17 km s^{-1}. The second phase lasted up to 09:00 UT. Another interesting feature observed in this phase was the observation of oscillations during the filament eruption. This oscillatory behaviour was observed throughout the second phase. Finally, the third phase started, where the eruption speed was maximum of $\sim$ 138 km s^{-1}. The eruption of this filament produced a large partial halo CME.

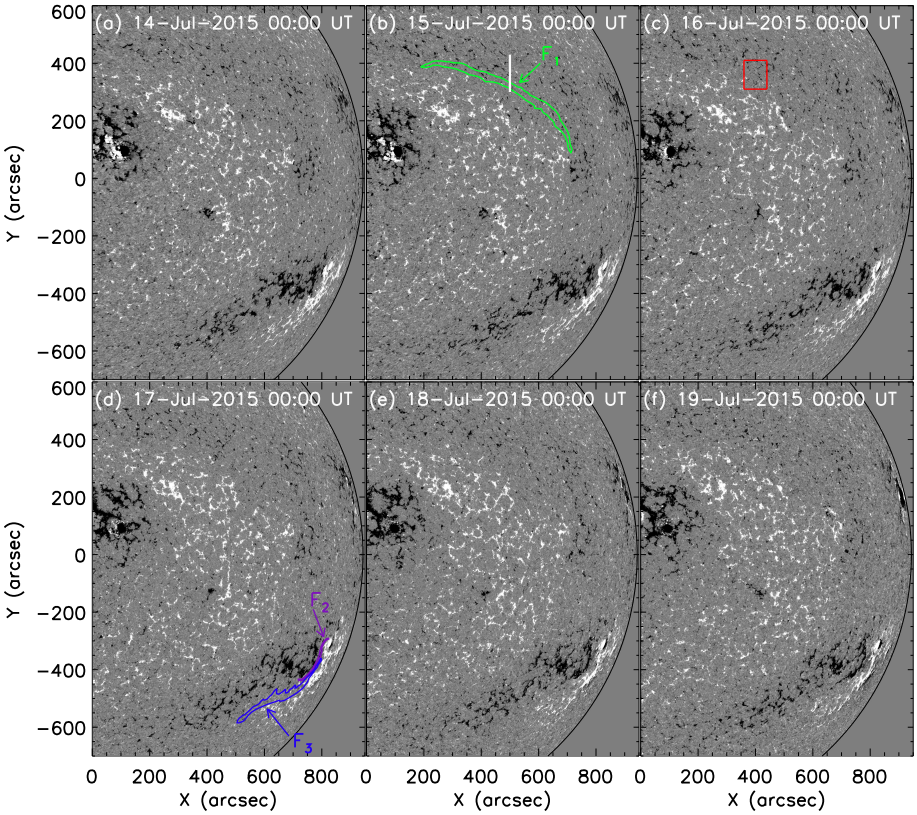

Figure 7. Evolution of HMI LOS magnetic field during 14 – 19 July 2015 before the onset of the eruption. The locations of the filaments are overlaid in 'b' and 'd' panel of the figure. The white line in panel 'b' denotes the slit position, used for time-slice plot shown in Figure 9. The red box in panel 'c' marks the region used for magnetic flux analysis, shown in Figure 10. See also the accompanying movie.

3.3. Magnetic field analysis

To examine the photospheric magnetic field evolution we performed a careful inspection of the HMI magnetic field movies (see online movies) and found regions of small-scale flux emergence/cancellation at the F_1 filament site and much more flux cancellation at the location of F_2 and F_3 filaments.

Figure 7 presents the magnetic field evolution between 14 – 19 July 2015, with overploted the filament positions in panels 'b' and 'd'. The analyzed region, which is located at $\sim 41°$ from the central meridian, is marked by red box in panel 'c' of the Figure 7.

The photospheric magnetic fields shown in Figure 7 indicate that F_1 is lying down along the neutral line. The F_1 eastern part is ending in the bipolar region (500″, 371″), where at 00:42 UT an emerging flux (EF) was observed. At the same time *i.e.* at 00:42 UT, the filament F_1 started to erupt and part of its material lifted up in northwest direction up to 03:20 UT, when it escaped the

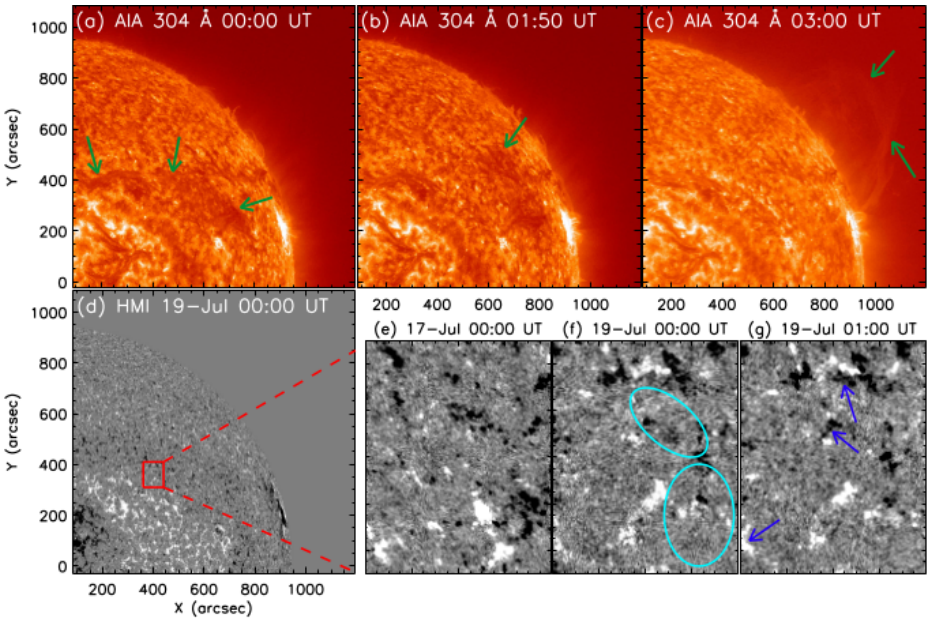

Figure 8. (a)–(c) F_1 eruption evolution in AIA 304 Å . The green arrows point to the rising F_1 filament. (d) The co-aligned HMI LOS magnetic field image. (e)–(g) The close-up magnetic field evolution, zoomed into the area shown as red rectangle in (d): Magnetic field quite state (e); During the magnetic field pre-eruptive state the cancellation is shown by cyan ellipses in panel (f) and flux emergence is shown by blue arrows in panel (g).

AIA FOV. Moreover, between 01:30 UT and 03:20 UT we observed a part of F_1 material to move down in southward direction up to the F_2 position. In Figure 8 are shown a co-aligned image of AIA 304 (with a rising F_1) and LOS HMI magnetic field image. The close-up magnetic field evolution, zoomed into the area shown as red rectangle Figure 7 (c), is presented for the magnetic field quiet state Figure 8 (e), while during its pre-eruptive state (Figure 8 f, g), the cancellations and emergence of the magnetic field are shown.

The emerging flux close to the F_1 location is well visible in time-distance plot, shown in Figure 9. The slit position is shown in Figure 7(b) by white vertical line. The time variations of both positive and negative LOS magnetic fluxes in the cancellation region, estimated in the box area shown in Figure 7(c) from 23:19 UT on 18 July to 10:19 UT on 19 July, are presented in Figure 10. During the pre-eruptive phase of the F_1 eruption, the positive flux steeply decreased up to 00:00 UT, when was the start time of EF close the eastern F_1 footpoint (see Figure 8) Then, it undergone a small increasing up to the F_1 eruption onset. After the eruption, the positive flux gradually decreased with an amplitude oscillations. During the pre-eruptive phase, the negative magnetic flux showed a similar behavior. After the eruption it gradually decreased with an amplitude oscillations up to 04:30 UT and then the negative flux steeply decreased up to 09:00 UT. In the pre-eruption phase (*i.e.* 18 July 23:30 UT – 19 July 00:00 UT), the decrease in both positive and negative fluxes can be considered as evidence of flux cancellation at the neutral line of the filament (Sterling *et al.*, 2010;

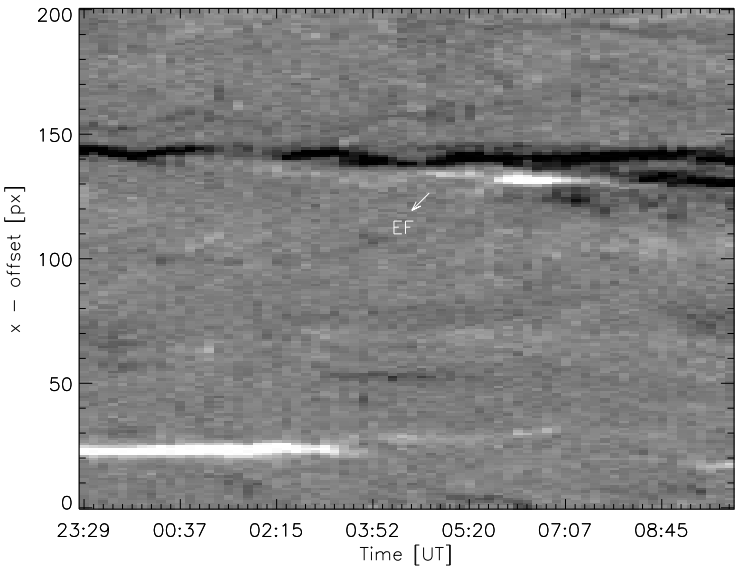

Figure 9. Time-distance plot, showing the emerging flux close to the F_1 location. The slit position is shown in Figure 7(b).

Green, Kliem, and Wallace, 2011). Hence, there were sites of flux emergence and cancellation in and around the filament, influencing its stability.

The pre-eruptive EUV brightening was observed in the vicinity of the filament channel prior to the F_1 eruption, between 23:40 UT on July 18 and 00:50 UT on July 19 (see Figure 2). This pre-eruptive brightening represents series of small-scale patches aligned to the neutral line beneath the filament. The brightening was visible not only in 304 Å and 171 Å channels, but also in the high temperature AIA channels 193 Å, 131 Å and 94 Å. The flux cancellations presented prior to the F_1 eruption are probably caused by the slow magnetic reconnections between the moving negative fluxes and its nearby positive fluxes (Wang and Shi, 1993), which would lead to some small-scale activities observed as the EUV brightenings, for example (Chen *et al.*, 2019).

The pre-eruptive brightening in the vicinity of F_2 and F_3 was visible in all AIA channels. In Figure 11 the evolution of EUV brightening is presented in three high temperature AIA channels, such as 171 Å, 193 Å and 211 Å. We found that the first indications of the pre-eruptive brightening enhancement occurred after 02:40 UT. This brightening enhancement was slow and fragmented, i.e. in different small-scale locations of filament vicinity along the PIL. Such brightening could be caused by a slow reconnection acting in the course of the flux cancellations process during the pre-eruptive phase (Chen *et al.*, 2019). After 04:00 UT significant and dynamic changes in the brightening occurred. The brightening enhancement covered the all filament vicinity, rapidly increasing and reaching a peak at 04:30 UT, i.e. when an extreme brightening was observed in some

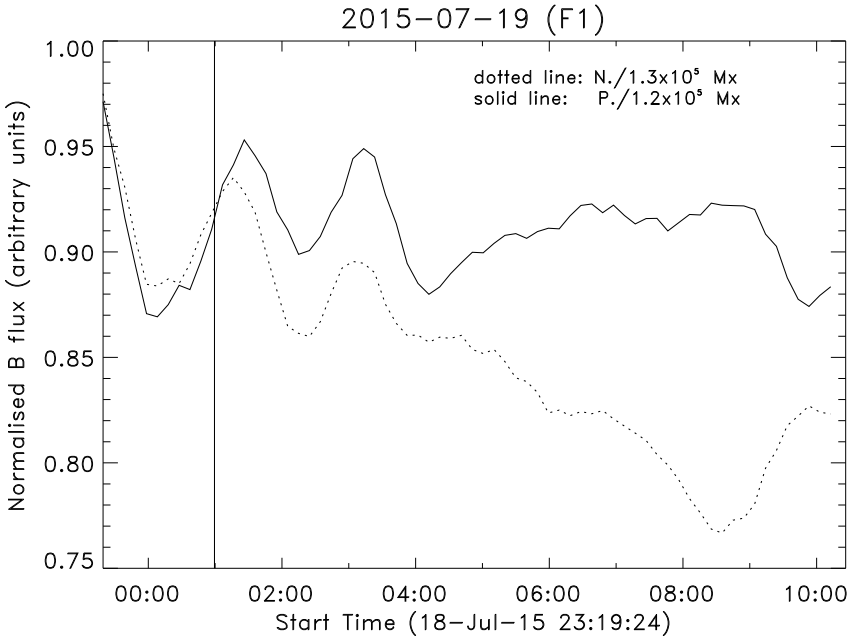

Figure 10. Light curves of the normalised (to the maximum) magnetic fluxes, obtained from the red box, shown in Figure 7 c. The vertical line represents the onset time of F_1 rising.

parts of the interacting and merging F_2 and F_3 flux ropes (FRs). Afterward, the brightening rapidly decreased and after 05:00 UT, when the F_2–F_3 compound flux rope rose up, it returned to the initial rate.

4. Discussion and Summary

We analyze the sympathetic eruption of three filaments observed on 19 July 2015. The filament F_1 was a quiet filament located in the northern hemisphere, while the F_2 and F_3 filaments were located in the active region NOAA AR 12384 in the southern hemisphere. The main results of this study are summarized as follows:

- All the eruptions are sympathetic and are associated with CMEs.
- The time-distance analysis and the morphology of the filaments suggest that filament F_1 triggered F_2, which consequently triggered F_3.
- We found that flux emergence/cancellation plays an important role in the observed filament eruption. We suggest that the emergence/cancellation of magnetic fluxes near the F_1 causes the flux rope to rise.

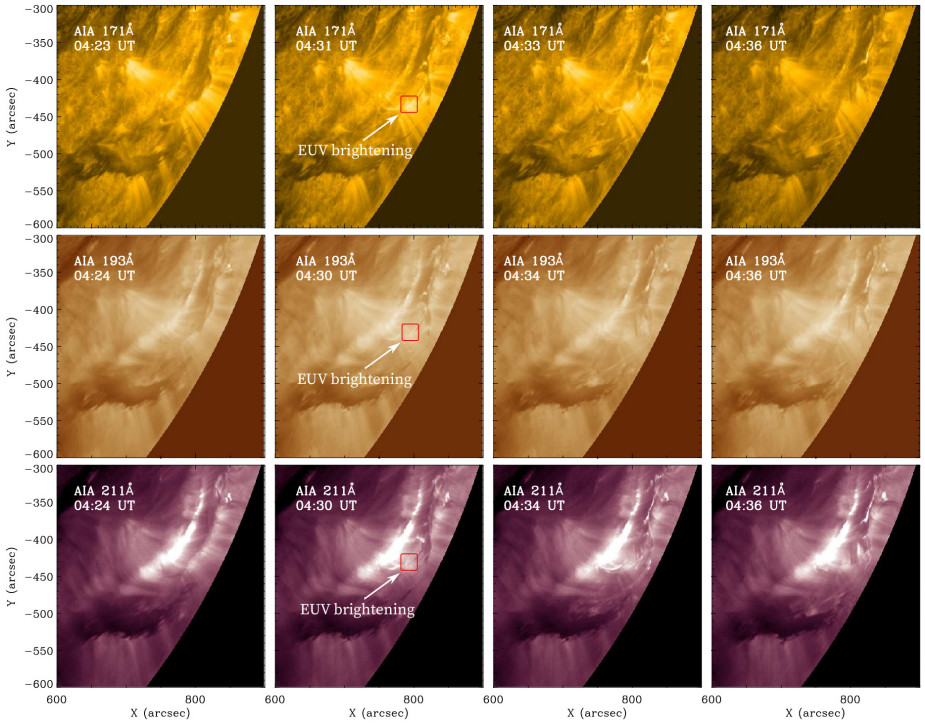

Figure 11. Evolution of the EUV brightening in the vicinity of F_2 and F_3 filaments in three different AIA channels. Top panel: AIA 171 Å; middle panel: AIA 193 Å; bottom panel: AIA 211 Å. The 211 images are brightened with accent to the ribbon flare. All data are derotated up to 04:58 UT.

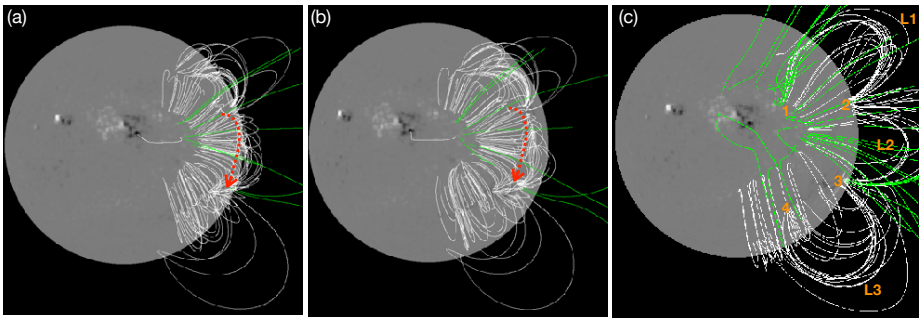

Figure 12. PFSS extrapolation on 19 July 2015 at 00:00 UT (a). In panel (b) the PFSS extrapolation is shown from different view, rotated to the top of the moving channel. The direction of ejected F_1 material towards F_2 and F_3 location is shown by red dashed arrow. The two filament locations are connected by different loop systems and represented by L_1, L_2, and L_3 in panel 'c' of the figure.

- In addition to these processes, the material movement from F_1 to the F_2-F_3 location can additionally contribute to the F_2–F_3 compound FR destabilization.

- Our observations can be explained by the combination of models proposed by Ding, Hu, and Wang (2006) and Török *et al.* (2011).

Our analysis of the magnetic flux evolution beneath the eastern part of filament F_1 suggest that the flux emergence via magnetic flux cancellation caused F_1 destabilization. An important feature of the F_1, F_2 and F_3 evolution is the pre-eruptive EUV brightening. During the slow rise of filaments F_2 and F_3 an extreme EUV brightening occurred at some parts of the merging F_2 and F_3 (see Figure 11), that suggests a sequence of partial merging episodes. Such brightening could be caused by the plasma heating, due to the energy released from reconnection site, below the rising prominence (Su *et al.*, 2015).

The merging of F_2 and F_3 is due to the stronger instability of the lower F_2 FR in comparison to those of the upper F_3 FR, which according to Kliem *et al.*, 2014 is the condition for FRs merging mechanism to work. Another condition for the merging of the two filaments could be the magnetic flux cancellation between them. Such a condition for the two filament merging was discussed in the study of Chandra *et al.* (2011). They found that the continuous decrease in the magnetic flux between the filaments brings them close to each other for the merging. Later the same observations were simulated by Török *et al.* (2011) who confirmed these observational results.

About the eruption of F_2–F_3 compound FR, it is important to note the suggestion of Aulanier *et al.*, 2010 that flux cancellation and tether-cutting reconnection are a key pre-eruption mechanisms for the buildup and the slow rise of an MFR, but they cannot trigger solar eruption alone. Moreover, the authors suggest the torus instability as an additional destabilizing mechanism.

Another event that can also cause significant EUV brightening and subsequently to affect the F_2 stability is the inflow of F_1 material in the vicinity of F_2. Such a brightening is considered as an observational signature of falling material and its impact on the solar atmosphere (Gilbert *et al.*, 2013). Moreover, the fluid instabilities associated with the falling material were described recently by Innes *et al.*, 2012. There are two mechanisms, compression and reconnection, that can explain the EUV brightening observed in the SDO/AIA channels. Which of them is responsible or dominant, depends on the amount of the energy associated with the observed emission. As Gilbert *et al.*, 2013 pointed out, although the dominance of one mechanism over the other, both are likely occurring, since the falling material undoubtedly carries frozen-in magnetic flux. Therefore, the falling F_1 material in the vicinity of F_2 could be considered as additional mechanism that also facilitates the destabilization of F_2 filament. Moreover, this event provides an observational evidence for the physical linkage between the three eruptions.

Ding, Hu, and Wang (2006) proposed the 2.5D MHD model for the sympathetic eruption. They consider three FRs embedded in different arcade system and same large scale magnetic field contributes for all these FRs systems. When one FR becomes unstable (or erupted) due to catastrophic behaviour, the global

shared magnetic filed changes significantly for the unfinished FRs. As a result, these undisturbed FRs becomes catastrophically unstable and erupt.

The 3D MHD simulation was proposed by Török *et al.* (2011) for the sympathetic eruption of 1 August 2010. According to their model two mechanism are proposed. The first FR erupted due to the converging flow and the another two FR are initiated by the removal of magnetic flux above the FRs due to the magnetic reconnection triggered by first FR eruption.

In current observations, we believe that the first filament F_1 eruption could allow to reconnect the open field lines with the overlying field lines of F_2 and F_3 filament system. As a result of this the magnetic tension above F_2 and F_3 filament becomes weaker and they start to erupt. After comparing our reported observations with the above models, we believe our events can be explained by the combination of both above discussed models.

To explain the possible scenarios of the observations, we have performed the PFSS extrapolation of the pohospheric magnetic filed. The result is presented in Figure 12. In panel (a) the PFSS extrapolation on 19 July 2015 at 00:00 UT is presented. In panel (b) the PFSS extrapolation is shown from different view, rotated to the top of the moving channel. Using this figure, we present the following explanation for the current eruption: The erupted part of the filament F_1 partially went through the open field lines (shown by green color in the figure) in north-west direction, which later observed as a CME. Major part of the erupted filament F_1 went towards the location of filaments F_2 through the channel of closed field lines (shown by red arrow). This part disturbed the filament F_2 and allows it to erupt. Since the erupted material probably was channeled under the closed magnetic fields, the observed case can be similar to the scenario of Wang *et al.* (2016), *i.e.*, the filament (F_1) does not completely erupt under the closed field lines, but trigger the filament (F_2) nearby the open fields to erupt. Another scenario of the sympathetic eruption can be explained by panel 'c' of Figure 12. In this scenario filament F_1 and F_2-F_3 are connected by following set of loops: Loop system L_1 connects site '1' to site '2', Loop system L_2 connects site '2' to site '3' and similarly site '3' is connected to site '4' by loops L_3. The erupted material from F_1 went towards F_2-F_3 through loop system L_1, L_2, and L_3 and it disturbed the stability of filaments F_2 and F_3. As a result of this disturbance, filament F_2 and F_3 erupted.

Disclosure of Potential Conflicts of Interest The authors declare that they have no conflicts of interest.

Acknowledgments We are thankful to the referee for the constructive comments and suggestions. We acknowledge the open data policy of SDO, SOHO and GONG missions. This work is supported by the Bulgarian Science Fund and the Department of Science & Technology, Government of India Fund under Indo-Bulgarian bilateral project No. DST/INT/BLS/P-11/2019 and KP-06-India/14 (19 -Dec-2019). PD thank the CSIR, New Delhi, for providing the research fellowship.

References

Aulanier, G., DeVore, C.R., Antiochos, S.K.: 2002, Prominence Magnetic Dips in Three-Dimensional Sheared Arcades. *Astrophys. J. Lett.* **567**(1), L97. DOI. ADS.

Aulanier, G., DeVore, C.R., Antiochos, S.K.: 2006, Solar Prominence Merging. *Astrophys. J.* **646**(2), 1349. DOI. ADS.

Aulanier, G., Török, T., Démoulin, P., DeLuca, E.E.: 2010, Formation of Torus-Unstable Flux Ropes and Electric Currents in Erupting Sigmoids. *Astrophys. J.* **708**(1), 314. DOI. ADS.

Becker, U.: 1958, Beobachtungen von drei Eruptionen im weiβen Licht. Mit 5 Textabbildungen. *Zeitschrift für Astrophysik* **46**, 168. ADS.

Biesecker, D.A., Thompson, B.J.: 2000, Sympathetic flaring with BATSE, GOES, and EIT data. *Journal of Atmospheric and Solar-Terrestrial Physics* **62**(16), 1449. DOI. ADS.

Brueckner, G.E., Howard, R.A., Koomen, M.J., Korendyke, C.M., Michels, D.J., Moses, J.D., Socker, D.G., Dere, K.P., Lamy, P.L., Llebaria, A., Bout, M.V., Schwenn, R., Simnett, G.M., Bedford, D.K., Eyles, C.J.: 1995, The Large Angle Spectroscopic Coronagraph (LASCO). *Solar Phys.* **162**(1-2), 357. DOI. ADS.

Chae, J.: 2001, Observational Determination of the Rate of Magnetic Helicity Transport through the Solar Surface via the Horizontal Motion of Field Line Footpoints. *Astrophys. J. Lett.* **560**(1), L95. DOI. ADS.

Chandra, R., Pariat, E., Schmieder, B., Mandrini, C.H., Uddin, W.: 2010, How Can a Negative Magnetic Helicity Active Region Generate a Positive Helicity Magnetic Cloud? *Solar Phys.* **261**(1), 127. DOI. ADS.

Chandra, R., Schmieder, B., Mandrini, C.H., Démoulin, P., Pariat, E., Török, T., Uddin, W.: 2011, Homologous Flares and Magnetic Field Topology in Active Region NOAA 10501 on 20 November 2003. *Solar Phys.* **269**(1), 83. DOI. ADS.

Chandra, R., Démoulin, P., Devi, P., Joshi, R., Schmieder, B.: 2021, Filament Eruption Driving EUV Loop Contraction and Then Expansion above a Stable Filament. *Astrophys. J.* **922**(2), 227. DOI. ADS.

Chen, H., Zheng, R., Li, L., Ma, S., Bi, Y., Yang, S.: 2019, Untwisting and Disintegration of a Solar Filament Associated with Photospheric Flux Cancellation. *Astrophys. J.* **871**(2), 229. DOI. ADS.

Cheng, X., Kliem, B., Ding, M.D.: 2018, Unambiguous Evidence of Filament Splitting-induced Partial Eruptions. *Astrophys. J.* **856**(1), 48. DOI. ADS.

Cheng, X., Zhang, J., Kliem, B., Török, T., Xing, C., Zhou, Z.J., Inhester, B., Ding, M.D.: 2020, Initiation and Early Kinematic Evolution of Solar Eruptions. *Astrophys. J.* **894**(2), 85. DOI. ADS.

Delannée, C., Aulanier, G.: 1999, Cme Associated with Transequatorial Loops and a Bald Patch Flare. *Solar Phys.* **190**, 107. DOI. ADS.

Devi, P., Démoulin, P., Chandra, R., Joshi, R., Schmieder, B., Joshi, B.: 2021, Observations of a prominence eruption and loop contraction. *Astron. Astrophys.* **647**, A85. DOI. ADS.

Ding, J.Y., Hu, Y.Q., Wang, J.X.: 2006, Catastrophic Behavior of Multiple Coronal Flux Rope System. *Solar Phys.* **235**(1-2), 223. DOI. ADS.

Gekelman, W., Lawrence, E., Van Compernolle, B.: 2012, Three-dimensional Reconnection Involving Magnetic Flux Ropes. *Astrophys. J.* **753**(2), 131. DOI. ADS.

Gibson, S.E.: 2018, Solar prominences: theory and models. Fleshing out the magnetic skeleton. *Living Rev. of Solar Phys.* **15**(1), 7. DOI. ADS.

Gibson, S.E., Fan, Y.: 2006, The Partial Expulsion of a Magnetic Flux Rope. *Astrophys. J. Lett.* **637**(1), L65. DOI. ADS.

Gilbert, H.R., Inglis, A.R., Mays, M.L., Ofman, L., Thompson, B.J., Young, C.A.: 2013, Energy Release from Impacting Prominence Material Following the 2011 June 7 Eruption. *Astrophys. J. Lett.* **776**(1), L12. DOI. ADS.

Gopalswamy, N., Yashiro, S., Akiyama, S.: 2007, Geoeffectiveness of halo coronal mass ejections. *Journal of Geophysical Research (Space Physics)* **112**(A6), A06112. DOI. ADS.

Gopalswamy, N., Shimojo, M., Lu, W., Yashiro, S., Shibasaki, K., Howard, R.A.: 2003, Prominence Eruptions and Coronal Mass Ejection: A Statistical Study Using Microwave Observations. *Astrophys. J.* **586**(1), 562. DOI. ADS.

Green, L.M., Kliem, B., Wallace, A.J.: 2011, Photospheric flux cancellation and associated flux rope formation and eruption. *Astron. Astrophys.* **526**, A2. DOI. ADS.

Harvey, J.W., Hill, F., Hubbard, R.P., Kennedy, J.R., Leibacher, J.W., Pintar, J.A., Gilman, P.A., Noyes, R.W., Title, A.M., Toomre, J., Ulrich, R.K., Bhatnagar, A., Kennewell, J.A.,

Marquette, W., Patron, J., Saa, O., Yasukawa, E.: 1996, The Global Oscillation Network Group (GONG) Project. *Science* **272**(5266), 1284. DOI. ADS.

Innes, D.E., Cameron, R.H., Fletcher, L., Inhester, B., Solanki, S.K.: 2012, Break up of returning plasma after the 7 June 2011 filament eruption by Rayleigh-Taylor instabilities. *Astron. Astrophys.* **540**, L10. DOI. ADS.

Jiang, Y., Yang, J., Wang, H., Ji, H., Liu, Y., Li, H., Li, J.: 2014, Interaction and Merging of two Sinistral Filaments. *Astrophys. J.* **793**(1), 14. DOI. ADS.

Joshi, N.C., Srivastava, A.K., Filippov, B., Uddin, W., Kayshap, P., Chandra, R.: 2013, A Study of a Failed Coronal Mass Ejection Core Associated with an Asymmetric Filament Eruption. *Astrophys. J.* **771**(1), 65. DOI. ADS.

Joshi, N.C., Srivastava, A.K., Filippov, B., Kayshap, P., Uddin, W., Chandra, R., Prasad Choudhary, D., Dwivedi, B.N.: 2014, Confined Partial Filament Eruption and its Reformation within a Stable Magnetic Flux Rope. *Astrophys. J.* **787**(1), 11. DOI. ADS.

Khan, J.I., Hudson, H.S.: 2000, Homologous sudden disappearances of transequatorial interconnecting loops in the solar corona. *Geophys. Res. Lett.* **27**(8), 1083. DOI. ADS.

Kliem, B., Török, T., Titov, V.S., Lionello, R., Linker, J.A., Liu, R., Liu, C., Wang, H.: 2014, Slow Rise and Partial Eruption of a Double-decker Filament. II. A Double Flux Rope Model. *Astrophys. J.* **792**(2), 107. DOI. ADS.

Kumar, P., Srivastava, A.K., Filippov, B., Erdélyi, R., Uddin, W.: 2011, Multiwavelength Observations of a Failed Flux Rope in the Eruption and Associated M-Class Flare from NOAA AR 11045. *Solar Phys.* **272**(2), 301. DOI. ADS.

Labrosse, N., Heinzel, P., Vial, J.-C., Kucera, T., Parenti, S., Gunár, S., Schmieder, B., Kilper, G.: 2010, Physics of Solar Prominences: I—Spectral Diagnostics and Non-LTE Modelling. *Space Sci. Rev.* **151**(4), 243. DOI. ADS.

Lemen, J.R., Title, A.M., Akin, D.J., Boerner, P.F., Chou, C., Drake, J.F., Duncan, D.W., Edwards, C.G., Friedlaender, F.M., Heyman, G.F., Hurlburt, N.E., Katz, N.L., Kushner, G.D., Levay, M., Lindgren, R.W., Mathur, D.P., McFeaters, E.L., Mitchell, S., Rehse, R.A., Schrijver, C.J., Springer, L.A., Stern, R.A., Tarbell, T.D., Wuelser, J.-P., Wolfson, C.J., Yanari, C., Bookbinder, J.A., Cheimets, P.N., Caldwell, D., Deluca, E.E., Gates, R., Golub, L., Park, S., Podgorski, W.A., Bush, R.I., Scherrer, P.H., Gummin, M.A., Smith, P., Auker, G., Jerram, P., Pool, P., Soufli, R., Windt, D.L., Beardsley, S., Clapp, M., Lang, J., Waltham, N.: 2012, The Atmospheric Imaging Assembly (AIA) on the Solar Dynamics Observatory (SDO). *Solar Phys.* **275**(1-2), 17. DOI. ADS.

Linton, M.G.: 2006, Reconnection of nonidentical flux tubes. *Journal of Geophysical Research (Space Physics)* **111**(A12), A12S09. DOI. ADS.

Liu, R., Wang, H., Alexander, D.: 2009, Implosion in a Coronal Eruption. *Astrophys. J.* **696**(1), 121. DOI. ADS.

Liu, Y., Webb, D.F., Zhao, X.P.: 2006, Magnetic Structures of Solar Active Regions, Full-Halo Coronal Mass Ejections, and Geomagnetic Storms. *Astrophys. J.* **646**(2), 1335. DOI. ADS.

Liu, Y., Hoeksema, J.T., Scherrer, P.H., Schou, J., Couvidat, S., Bush, R.I., Duvall, T.L., Hayashi, K., Sun, X., Zhao, X.: 2012, Comparison of Line-of-Sight Magnetograms Taken by the Solar Dynamics Observatory/Helioseismic and Magnetic Imager and Solar and Heliospheric Observatory/Michelson Doppler Imager. *Solar Phys.* **279**(1), 295. DOI. ADS.

Luna, M., Su, Y., Schmieder, B., Chandra, R., Kucera, T.A.: 2017, Large-amplitude Longitudinal Oscillations Triggered by the Merging of Two Solar Filaments: Observations and Magnetic Field Analysis. *Astrophys. J.* **850**(2), 143. DOI. ADS.

Mackay, D.H., Karpen, J.T., Ballester, J.L., Schmieder, B., Aulanier, G.: 2010, Physics of Solar Prominences: II—Magnetic Structure and Dynamics. *Space Sci. Rev.* **151**(4), 333. DOI. ADS.

Monga, A., Sharma, R., Liu, J., Cid, C., Uddin, W., Chandra, R., Erdélyi, R.: 2021, On the partial eruption of a bifurcated solar filament structure. *Mon. Not. Roy. Astron. Soc.* **500**(1), 684. DOI. ADS.

Moon, Y.-J., Choe, G.S., Park, Y.D., Wang, H., Gallagher, P.T., Chae, J., Yun, H.S., Goode, P.R.: 2002, Statistical Evidence for Sympathetic Flares. *Astrophys. J.* **574**(1), 434. DOI. ADS.

Morgan, H., Druckmüller, M.: 2014, Multi-Scale Gaussian Normalization for Solar Image Processing. *Solar Phys.* **289**(8), 2945. DOI. ADS.

Pesnell, W.D., Thompson, B.J., Chamberlin, P.C.: 2012, The Solar Dynamics Observatory (SDO). *Solar Phys.* **275**, 3. DOI. ADS.

Richardson, R.S.: 1936, Further Solar Observations in Connection with High-Frequency Radio Fadeouts. *Pub. Astron. Soc. Pac.* **48**(282), 122. DOI. ADS.

Richardson, R.S.: 1951, Characteristics of Solar Flares. *Astrophys. J.* **114**, 356. DOI. ADS.
Scherrer, P.H., Schou, J., Bush, R.I., Kosovichev, A.G., Bogart, R.S., Hoeksema, J.T., Liu, Y., Duvall, T.L., Zhao, J., Title, A.M., Schrijver, C.J., Tarbell, T.D., Tomczyk, S.: 2012, The Helioseismic and Magnetic Imager (HMI) Investigation for the Solar Dynamics Observatory (SDO). *Solar Phys.* **275**(1-2), 207. DOI. ADS.
Schmieder, B., Démoulin, P., Aulanier, G.: 2013, Solar filament eruptions and their physical role in triggering coronal mass ejections. *Adv. Space Res.* **51**(11), 1967. DOI. ADS.
Schmieder, B., Mein, N., Deng, Y., Dumitrache, C., Malherbe, J.-M., Staiger, J., Deluca, E.E.: 2004, Magnetic changes observed in the formation of two filaments in a complex active region: TRACE and MSDP observations. *Solar Phys.* **223**(1-2), 119. DOI. ADS.
Schmieder, B., Kim, R.S., Grison, B., Bocchialini, K., Kwon, R.Y., Poedts, S., Démoulin, P.: 2020, Low geo-effectiveness of fast halo CMEs related to the 12 X-class flares in 2002. *arXiv e-prints*, arXiv:2003.10777. ADS.
Schou, J., Scherrer, P.H., Bush, R.I., Wachter, R., Couvidat, S., Rabello-Soares, M.C., Bogart, R.S., Hoeksema, J.T., Liu, Y., Duvall, T.L., Akin, D.J., Allard, B.A., Miles, J.W., Rairden, R., Shine, R.A., Tarbell, T.D., Title, A.M., Wolfson, C.J., Elmore, D.F., Norton, A.A., Tomczyk, S.: 2012, Design and Ground Calibration of the Helioseismic and Magnetic Imager (HMI) Instrument on the Solar Dynamics Observatory (SDO). *Solar Phys.* **275**, 229. DOI. ADS.
Schrijver, C.J., Title, A.M.: 2011, Long-range magnetic couplings between solar flares and coronal mass ejections observed by SDO and STEREO. *Journal of Geophysical Research (Space Physics)* **116**(A4), A04108. DOI. ADS.
Schrijver, C.J., Elmore, C., Kliem, B., Török, T., Title, A.M.: 2008, Observations and Modeling of the Early Acceleration Phase of Erupting Filaments Involved in Coronal Mass Ejections. *Astrophys. J.* **674**(1), 586. DOI. ADS.
Sterling, A.C., Chifor, C., Mason, H.E., Moore, R.L., Young, P.R.: 2010, Evidence for magnetic flux cancelation leading to an ejective solar eruption observed by Hinode, TRACE, STEREO, and SoHO/MDI. *Astron. Astrophys.* **521**, A49. DOI. ADS.
Su, Y., van Ballegooijen, A., McCauley, P., Ji, H., Reeves, K.K., DeLuca, E.E.: 2015, Magnetic Structure and Dynamics of the Erupting Solar Polar Crown Prominence on 2012 March 12. *Astrophys. J.* **807**(2), 144. DOI. ADS.
Török, T., Panasenco, O., Titov, V.S., Mikić, Z., Reeves, K.K., Velli, M., Linker, J.A., De Toma, G.: 2011, A Model for Magnetically Coupled Sympathetic Eruptions. *Astrophys. J. Lett.* **739**(2), L63. DOI. ADS.
van Ballegooijen, A.A., Martens, P.C.H.: 1989, Formation and Eruption of Solar Prominences. *Astrophys. J.* **343**, 971. DOI. ADS.
Wang, H., Ji, H., Schmahl, E.J., Qiu, J., Liu, C., Deng, N.: 2002, Sudden Disappearance of a Small Sunspot Associated with the 2002 February 20 M2.4 Flare. *Astrophys. J. Lett.* **580**(2), L177. DOI. ADS.
Wang, J., Shi, Z.: 1993, The Flare-Associated Magnetic Changes in an Active Region - Part Two. *Solar Phys.* **143**(1), 119. DOI. ADS.
Wang, R., Liu, Y.D., Zimovets, I., Hu, H., Dai, X., Yang, Z.: 2016, Sympathetic Solar Filament Eruptions. *Astrophys. J. Lett.* **827**(1), L12. DOI. ADS.
Wheatland, M.S., Craig, I.J.D.: 2006, Including Flare Sympathy in a Model for Solar Flare Statistics. *Solar Phys.* **238**(1), 73. DOI. ADS.
Zhukov, A.N., Veselovsky, I.S.: 2007, Global Coronal Mass Ejections. *Astrophys. J. Lett.* **664**(2), L131. DOI. ADS.